Chemical Science

ROYAL SOCIETY OF CHEMISTRY

EDGE ARTICLE

View Article Online
View Journal | View Issue

Cite this: *Chem. Sci.*, 2024, **15**, 17937

All publication charges for this article have been paid for by the Royal Society of Chemistry

Crystal engineering of a new platform of hybrid ultramicroporous materials and their C_2H_2/CO_2 separation properties†

Daniel J. O'Hearn,‡[a] Debobroto Sensharma, ‡[a] Asif Raza, ‡[a] Andrey A. Bezrukov, [a] Matthias Vandichel, *[a] Soumya Mukherjee *[ab] and Michael J. Zaworotko *[ab]

Hybrid ultramicroporous materials (HUMs) comprised of combinations of organic and inorganic linker ligands are a leading class of physisorbents for trace separations involving C1, C2 and C3 gases. First generation HUMs are modular in nature since they can be self-assembled from transition metal cations, ditopic linkers and inorganic "pillars", as exemplified by the prototypal variant, **SIFSIX-3-Zn** (**3** = pyrazine, **SIFSIX** = SiF_6^{2-}). Conversely, HUMs that utilise chelating ligands such as ethylenediamine derivatives are yet to be explored as sorbents. Herein, we report the structures and sorption properties of two HUMs based upon the chelating ligand N^1,N^2-bis(pyridin-4-ylmethyl)ethane-1,2-diamine (**enmepy**), $[Zn(\textbf{enmepy})(SiF_6)]_n$ (**SIFSIX-24-Zn**) and $[Zn(\textbf{enmepy})(SO_4)]_n$ (**SOFOUR-2-Zn**). These HUMs are isostructural and exhibit high C_2H_2 uptakes of 85 $cm^3\ g^{-1}$ (3.79 mmol g^{-1}) and 79 $cm^3\ g^{-1}$ (3.52 mmol g^{-1}), and C_2H_2/CO_2 IAST selectivities of 7.4 and 8.1 (1 bar, 1 : 1 mixture, 298 K), respectively. Dynamic column breakthrough experiments resulted in separation factors of 5.26 and 2.05, and CO_2 effluent purities of 99.991 and 99.989%, respectively. Temperature programmed desorption experiments at 60 °C resulted in rapid desorption of CO_2, followed by fuel grade C_2H_2 (>98%), affording productivities of 9.45 and 7.96 L kg^{-1} and maximum C_2H_2 outlet purities of 99.92% and 99.66%, respectively. This study introduces the use of diamine chelating ligands in HUMs for gas separations through two parent sorbents that are prototypal for families of related materials, one of which, **SOFOUR-2-Zn**, uses the earth-friendly sulfate anion as a pillar.

Received 8th May 2024
Accepted 26th September 2024

DOI: 10.1039/d4sc03029j

rsc.li/chemical-science

Introduction

The first studies that confirmed permanent porosity in porous coordination networks (PCNs)[1–3] spawned intense interest in study of PCNs[4,5] for their potential utility for gas separations including purification of light hydrocarbons.[6–9] One class of PCN, hybrid ultramicroporous materials (HUMs), is comprised of inorganic and organic linker ligands and can exhibit highly selective physisorption.[10] Their performance can be attributed to their ultramicroporous (≤7.0 Å) nature, which results in tight sorbate binding, and the strong electrostatics of the inorganic anions that line the pores,[11] in effect creating a high density of highly selective binding sites.[5] The prototypal HUM, $[Zn(SiF_6)(pyz)_2]_n$ (**SIFSIX-3-Zn**),[12] is comprised of an N-donor linker ligand, pyrazine (**3**), that links Zn^{2+} cations to form a cationic 2D square lattice topology, **sql**, network and SiF_6^{2-} (**SIFSIX**) anions that pillar the **sql** nets to form a 3D primitive cubic, **pcu**, topology network. **SIFSIX-3-Zn** was found to offer exceptional trace CO_2 capture properties over N_2 and CH_4,[10] and its inherent modularity enabled systematic fine-tuning of composition through substitution of the metal cation, organic linker ligand and/or the **SIFSIX** pillar, affording improvements in stability and performance.[10,13,14] Second generation HUMs pillared by **SIFSIX** and other MF_6^{2-} anions (M = Si, Ge, Sn, Ti, Zr) belong to the **MFSIX** platform.[15] Other HUM platforms have been based on different inorganic pillars, including **DICRO** ($Cr_2O_7^{2-}$),[16,17] **FOXY** ($NbOF_5^{2-}$),[18,19] **MFFIVE** (AlF_5^{2-}),[20] **mmo** topology nets (CrO_4^{2-},MoO_4^{2-}, WO_4^{2-}),[21] and, most recently, **SOFOUR** (SO_4^{2-}).[22]

A potential application for HUMs is acetylene (C_2H_2) purification. C_2H_2 is typically produced *via* oxidative coupling of CH_4 with CO_2 as a by-product.[9] Since C_2H_2 and CO_2 have the same kinetic diameter of 3.3 Å and similar boiling/sublimation points of 188.4 and 194.7 K, respectively,[5,6] sorptive separation is

[a]*Department of Chemical Sciences, Bernal Institute, University of Limerick, Limerick V94 T9PX, Ireland. E-mail: matthias.vandichel@ul.ie; soumya.mukherjee@ul.ie; xtal@ul.ie*

[b]*SSPC, Science Foundation Ireland Research Centre for Pharmaceuticals, University of Limerick, Limerick V94 T9PX, Ireland*

† Electronic supplementary information (ESI) available: Synthesis, gas sorption, modelling details, crystallographic information. CCDC 2206134. For ESI and crystallographic data in CIF or other electronic format see DOI: https://doi.org/10.1039/d4sc03029j

‡ These authors contributed equally to this work.

challenging. Industrially, purification is typically achieved using organic solvents, which is inefficient and requires multiple steps to reach the required levels of purity. HUMs such as **SIFSIX-dps-Cu**,[23] **UTSA-300a** [24] and **DICRO-4-Ni-i** [25] selectively adsorb C_2H_2 *via* strong C_2H_2 binding sites in which F atoms serve as hydrogen bond acceptors, particularly when spaced optimally (*ca.* 7 Å) to interact with both ends of a C_2H_2 molecule.[6] Recently, the linker ligand bpe, 1,2-bis(4-pyridyl)ethane, afforded a layered flexible HUM, **sql-SIFSIX-bpe-Zn**, the activated phase of which, **sql-SIFSIX-bpe-Zn-β**, set a new benchmark for C_2H_2 adsorption enthalpy (Q_{st}) of 67.5 kJ mol^{-1}.[26] This strong binding was attributed to induced fit of C_2H_2 molecules by enzyme-like adaptable sorbent binding sites and **sql-SIFSIX-bpe-Zn-β** was found to be highly C_2H_2-selective over both ethylene and CO_2.

Although families of pillared HUMs composed of linear or angular ditopic linker ligands are the most commonly studied HUM variants, other ligand types are possible. HUMs with 4,6-connected **fsc** topology are composed of tetratopic ligands where the ligand serves as a 4-c node and the metal ion serves as a 6-c node. Examples of ligands and their respective **fsc** topology HUMs are as follows: metalloligand $[Cu_2(3\text{-(pyridin-4-yl) acrylate})_4]$ in **fsc-2-SIFSIX**;[27] tetra-(pyridin-4-yl)porphyrin in **CPM-131**;[28] "FTPFs" **Cu-Nb-M** (M = Zn, Fe, Ni);[29] 1,2,4,5-tetra(pyridin-4-yl)benzene (tepb) in **ZJU-280** (**SIFSIX-22-Cu**),[30] **SIFSIX-22-Zn**,[22,31] **SOFOUR-1-Zn**,[22] and **TIFSIX-Cu-TPB** (**TIFSIX-6-Cu**).[32] These materials have been studied for CO_2 capture,[27] electrocatalysis,[29] C_2H_2/C_2H_4 separation,[30] and C_2H_2/CO_2 separation.[22,26] Since the ligand serves as a 4-c node, such PCNs are also amenable to pillar substitution as exemplified by replacement of the **SIFSIX** pillar in **SIFSIX-22-Zn** by SO_4^{2-} (**SOFOUR**) in **SOFOUR-1-Zn** [22] and **SOFOUR-DPDS-Ni** (4-DPDS = 4,4′-dipyridyldisulfide),[33] and the use of other fluorinated pillars, *e.g.* TiF_6^{2-}, SnF_6^{2-}, GeF_6^{2-}, ZrF_6^{2-} and TaF_7^{2-}, while retaining **fsc** topology.[34] The SO_4^{2-} pillar has also been used in HUMs such as $CuSO_4(1,4\text{-bin})_{1.5}$ (1,4-bin = 1,4-bisimidazole naphthalene),[35] and **SOFOUR-TEPE-Zn** (TEPE = 1,1,2,2-tetra(pyridin-4-yl) ethene).[36]

Nevertheless, the availability of linker ligands suitable for HUMs remains somewhat limited in scope and derivatives of chelating ligands such as ethylenediamine (**en**), which represent a potentially inexpensive and versatile class of ligand, are to our knowledge unexplored. This is despite **en** and its derivatives representing 7.27% (55 046 entries) of coordination compounds archived in the Cambridge Structural Database (CSD version 5.45, September 2024).[37] In this contribution, we report a successful crystal engineering approach to preparing the prototypal members of two HUM platforms comprising a pyridyl functionalised chelating **en** ligand, **enmepy**, and their sorption properties in the context of C_2H_2/CO_2 gas separations.

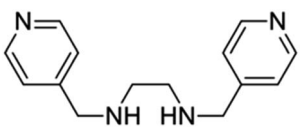

enmepy

Results and discussion

CSD analysis

In order to design and characterise new HUM platforms based on **en** derivatives, we first looked for reports of **en** chelates pillared by MF_6 anions (M = Si, Ge, Sn, Ti, Zr, Hf). Database mining of the CSD for coordination compounds containing both an **en** (or derivative) chelate and a coordinated **MFSIX** anion afforded just five hits (Table S1 and Fig. S1a†): two ZrF_6^{2-} complex anions $[[(ZrF_6)_2(ZrF_5(OH_2))_2]^{6-}$ and $[(ZrF_6)_2]^{4-}$); three 1D chains involving **SIFSIX** or TiF_6^{2-} (**TIFSIX**) linkers ($[Cu(\mathbf{en})_2(SiF_6)]_n$ and $[Cu(\mathbf{en})_2(TiF_6)]_n$). No apparent porosity was present or studied in these compounds.[38,39] This lack of sorption candidates prompted us to look at the earth-friendly inorganic pillar **SOFOUR** and our search (Fig. S1b†) resulted in 25 hits (20 distinct compounds, Table S2;† corresponding to chelating ligands listed in Fig. S2†). $[Cu(\mathbf{en})(OH_2)_2(SO_4)]_n$ and $[Zn(\mathbf{en})_2(SO_4)]_n$ are 1D chains with no apparent or permanent porosity.[40–45] However, **$[Zn(enmepy)(SO_4)]_n$** (CSD refcode ZOMNOG, hereinafter referred to as **SOFOUR-2-Zn**) is composed of the chelating **en** derivative N^1,N^2-bis(pyridin-4-ylmethyl)ethane-1,2-diamine (**enmepy**) and Zn^{2+} cations that form a **sql** network pillared by **SOFOUR** to afford a 3D **pcu** network. Even though **SOFOUR-2-Zn** contains 1D ultramicropores, no gas sorption data was reported.[46] We then searched for other structures containing **enmepy** chelates that form **sql** nets similar to **SOFOUR-2-Zn**. This search, which used the query in Fig. S3,† afforded 62 hits, manual inspection of which revealed 31 **sql** nets (see Table S3†). The majority (22) are not pillared, with axial positions metal cations coordinated by terminal ligands. The remaining entries were found to be pillared by either 1,4-benzenedicarboxylate derivatives,[47,48] MO_4^{2-} (M = Cr, Mo) or, in the case of **SOFOUR-2-Zn**, **SOFOUR**.[46] The earth friendly characteristics of **SOFOUR** over CrO_4^{2-} and MoO_4^{2-}, motivated us to characterise the sorption properties of **SOFOUR-2-Zn** along with its new **SIFSIX** variant, $[Zn(\mathbf{enmepy})(SiF_6)]_n$ (**SIFSIX-24-Zn**).

Crystal structures

SOFOUR-2-Zn was previously reported in 2014, crystallising in the monoclinic space group C2.[46] Each octahedral Zn^{2+} cation is chelated by amino groups of one **enmepy** and two pyridyl groups from two different **enmepy** ligands to fill its equatorial positions (Fig. 1a), thereby generating a 2D cationic network with **sql** topology (Fig. 1b). In each axial position, a **SOFOUR** anion serves as a pillar to adjacent **sql** layers so as to form a **pcu** topology network with an intermetallic distance between **sql** layers of 6.74 Å (Fig. 1c). The **sql** layers stack such that triangular 1D channels containing hydrate molecules run parallel to the crystallographic *c*-axis (Fig. 1b). The calculated void space is 40.9% of unit cell volume after removal of hydrate molecules (mercury contact surface, probe radius 1.2 Å).[49]

SIFSIX-24-Zn was prepared by reacting **enmepy** with $ZnSiF_6$. Crystals suitable for single crystal X-ray diffraction, SCXRD, were obtained by diffusion of a methanolic solution of **enmepy** layered onto an ethylene glycol solution of $ZnSiF_6$ (see ESI† for details). SCXRD data revealed that **SIFSIX-24-Zn** had crystallised

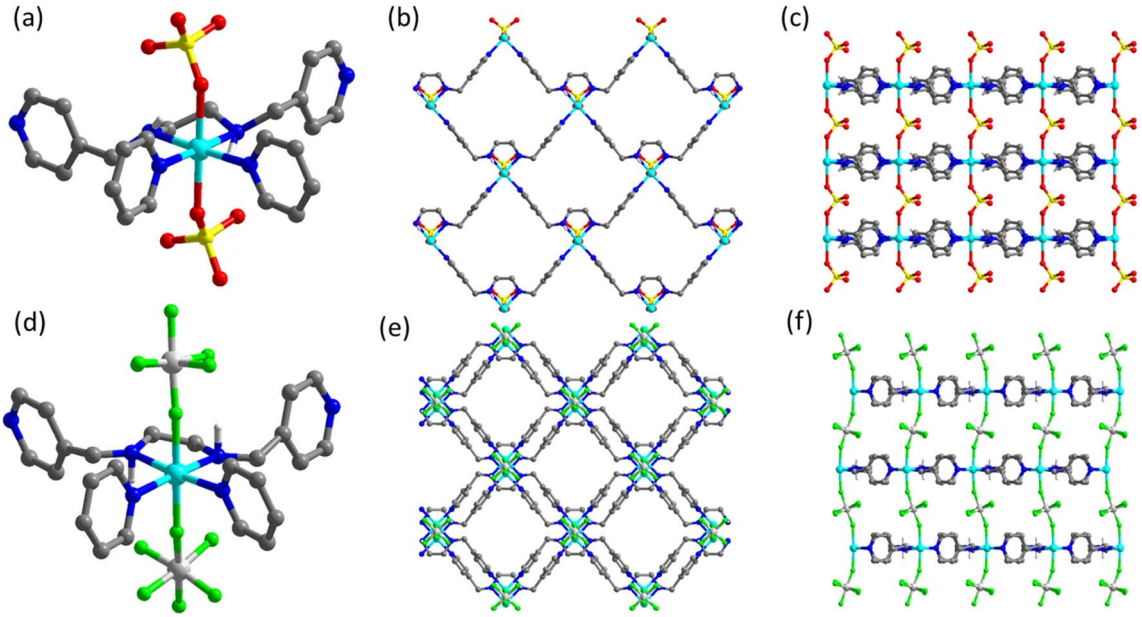

Fig. 1 Crystal structures of **SIFSIX-24-Zn** and **SOFOUR-2-Zn** (C–H atoms omitted for clarity, C = grey, H = white, N = blue, O = red, F = green, S = yellow, Si = light beige, Zn = cyan). (a) The octahedral coordination environment around Zn^{2+} in **SOFOUR-2-Zn**, (b) **SOFOUR-2-Zn** packing viewed along *a*-axis, (c) **SOFOUR-2-Zn** crystal packing viewed along *c*-axis, (d) the octahedral coordination environment around Zn^{2+} in **SIFSIX-24-Zn**. (e) **SIFSIX-24-Zn** crystal packing viewed along *b*-axis, (f) **SIFSIX-24-Zn** crystal packing viewed along *c*-axis.

in the chiral orthorhombic space group $C222_1$. The equatorial environment of the Zn^{2+} cations is similar to that of **SOFOUR-2-Zn** but the **SIFSIX** pillars form shorter bonds with the Zn cation at the axial positions (Zn–F = 2.148(5) Å *vs.* Zn–O = 2.223 Å, Fig. 1d). **SIFSIX-24-Zn** formed the same **sql** layers found in **SOFOUR-2-Zn**, resulting in the **pcu** network illustrated in Fig. 1e and f. The larger **SIFSIX** anion resulted in intermetallic distance between layers of 7.5759(16) Å (0.833 Å longer than **SOFOUR-2-Zn**, Fig. 1f). **SIFSIX-24-Zn** possesses similar 1D pores to **SOFOUR-2-Zn** but with diffuse electron density which was accounted for by the PLATON SQUEEZE[50] procedure in the final structure refinement. The void space (Mercury contact surface, probe radius 1.2 Å) was calculated to be 37.9% of unit cell volume. Further crystallographic details are presented in Table S4.†

In both **SOFOUR-2-Zn** and **SIFSIX-24-Zn**, all **enmepy** ligands within a **sql** layer orient in the same direction, precluding a crystallographic inversion centre. The stacking of **sql** layers differs between the two compounds. In **SOFOUR-2-Zn**, each layer is identical and orients in the same direction, whereas in **SIFSIX-24-Zn**, the layers alternate in direction and chirality and a pseudo centre of symmetry is present. Though this detail may seem inconsequential for gas adsorption, it impacts pore shape as becomes apparent when examining crystal packing (Fig. 1). The chirality of the **sql** layers formed by **enmepy** has been explored by Wen *et al.*, where homochiral batches of crystals could be obtained when using a homochiral template during crystallisation.[51–53] The **SIFSIX-24-Zn** crystal used for SCXRD study was found to be a racemic twin with a Flack parameter of 0.5 (Table S4†).[46,47]

Gas sorption

Pure gas sorption studies. In order to perform sorption studies, bulk samples of **SOFOUR-2-Zn** and **SIFSIX-24-Zn** were prepared by mixing methanolic solutions of **enmepy** with aqueous solutions of $ZnSO_4$ and $ZnSiF_6$, respectively, at room temperature, to obtain microcrystalline powders (see ESI† for synthetic details) with Powder X-ray diffraction (PXRD) patterns matching those calculated from SCXRD data (Fig. S4†). Thermogravimetric analysis (TGA) of **SOFOUR-2-Zn** and **SIFSIX-24-Zn** indicated loss of solvent molecules at 90 and 75 °C, respectively, and thermal stability up to approximately 300 °C and 200 °C, respectively (Fig. S5†). Following activation at 60 °C under dynamic vacuum, both materials exhibited type-I isotherms for CO_2 at 195 K, with saturation uptakes of 135 $cm^3\ g^{-1}$ and 178 $cm^3\ g^{-1}$, respectively (Fig. 2a), and apparent BET surface areas of 452 $m^2\ g^{-1}$ and 590 $m^2\ g^{-1}$, respectively (Fig. S6 and S7†). The Horvath–Kawazoe differential pore volume plots from 195 K CO_2 isotherms for both compounds were centred around 5.0 Å, classifying them as ultramicroporous (Fig. S8†). **SIFSIX-24-Zn** exhibited a minor inflection in the 195 K CO_2 isotherm in the absolute pressure range 100–200 mmHg. Similarly, **SOFOUR-2-Zn** revealed inflections at 350–400 mmHg in the CO_2 at 195 K isotherm (Fig. 2a), and at 5–10 mm Hg in the N_2 at 77 K isotherm (Fig. S9†). Such an inflection was not observed in the 273 K and 298 K CO_2 and C_2H_2 isotherms (Fig. S10 and S11†). At 298 K, the CO_2 uptakes of **SOFOUR-2-Zn** and **SIFSIX-24-Zn** at 1 bar were observed to be 41 $cm^3\ g^{-1}$ (1.78 mmol g^{-1}) and 40 $cm^3\ g^{-1}$ (1.79 mmol g^{-1}), respectively (Fig. 2b). The Q_{st} values for CO_2, 22.1 kJ mol^{-1} and 16.8 kJ mol^{-1}, respectively, at low loading (Fig. 2c and S12†) are

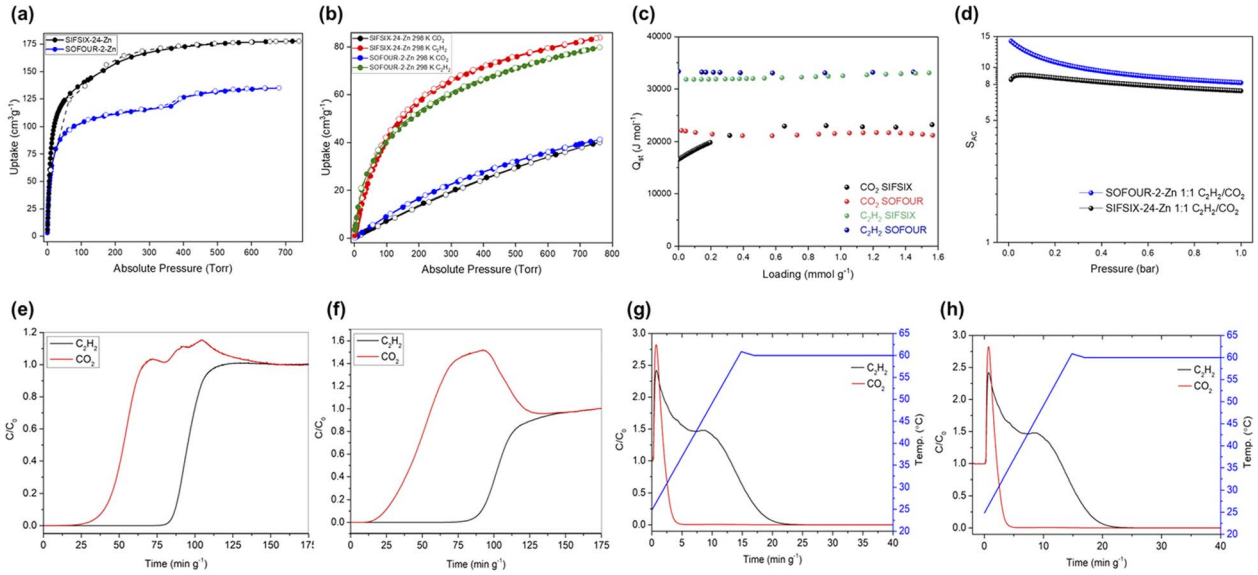

Fig. 2 Gas sorption properties of **SIFSIX-24-Zn** and **SOFOUR-2-Zn**: (a) 195 K CO_2; (b) 298 K C_2H_2 and CO_2, (c) Q_{st} for C_2H_2 and CO_2. (d) IAST selectivity for C_2H_2 over CO_2 at 298 K and 1 : 1(v/v) mixture; (e) breakthrough curve at 298 K for 1 : 1 C_2H_2/CO_2 mixture for **SOFOUR-22-Zn**; (f) breakthrough curve at 298 K for 1 : 1 C_2H_2/CO_2 mixture for **SIFSIX-24-Zn**; (g) temperature programmed desorption after breakthrough experiment for **SOFOUR-2-Zn**; (h) temperature programmed desorption after breakthrough experiment for **SIFSIX-24-Zn**.

exceptionally low. In contrast, the uptakes for C_2H_2 at 298 K were relatively high, 79 and 84 cm^3 g^{-1}, or 3.52 and 3.75 mmol g^{-1}, respectively (Fig. 2b), with Q_{st} values of 33.3 kJ mol^{-1} and 31.8 kJ mol^{-1}, respectively, at low loading.[54] Evidently both these sorbents exhibit a relatively high pure component uptake for C_2H_2 over CO_2 at 298 K, which is in the range that could break the usual trade-off between uptake and selectivity.[55,56] PXRD patterns measured after activation and adsorption experiments showed retention of the crystal structures of both materials (Fig. S13†).

Since single-component gas sorption isotherms revealed significantly higher C_2H_2 uptakes relative to CO_2, ideal adsorbed solution theory (IAST) was applied using the pyIAST Python package[57] to determine the selectivity for C_2H_2 in a 1 : 1 C_2H_2/CO_2 mixture, S_{AC}. We found moderate selectivities for **SOFOUR-2-Zn** and **SIFSIX-24-Zn** of 8.2 and 7.3 at 1 bar and 298 K, respectively (Fig. 2d and S14†). Although these selectivity numbers are lower than benchmark physisorbents such as **ZNU-1** (56.6),[58] **Zn$_2$(bpy)(btec)** (33.3),[59] **sql-16-Cu-NO$_3$-α** (27.8),[60] and **Ni$_3$(HCOO)$_6$** (22),[61] they are higher than HUMs such as **TIFSIX-2-Ni-i** (6.1),[62] and **NbOFFIVE-3-Ni** (6.0)[56] (see Table S5† for a list of leading C_2H_2/CO_2 selective PCNs). Combining both IAST selectivity and adsorption capacity recorded at 298 K, the separation potentials for both sorbents were found to be similar at 1 bar and 298 K: 0.78 mmol g^{-1} for **SOFOUR-2-Zn**, and 0.76 mmol g^{-1} for **SIFSIX-24-Zn** (Fig. S15†).

The water vapour sorption isotherm of **SOFOUR-2-Zn** reveals a sigmoidal adsorption profile with a total uptake approaching 30 wt% at 95% R.H. (relative humidity), followed by desorption with low hysteresis. In contrast, **SIFSIX-24-Zn** shows a sudden decrease in uptake at *ca.* 90% R.H., followed by high desorption hysteresis, typical of moisture-induced phase degradation (Fig. S16†). Accelerated stability tests conducted by incubating activated samples at 40 °C and 75% R.H. show retention of the porous phase of **SOFOUR-2-Zn** over 5 days, whereas significant new peaks are observed in **SIFSIX-24-Zn** within 90 hours of exposure (Fig. S17†), indicating that the SO_4^{2-} pillar enhances framework stability relative to SiF_6^{2-}.

Dynamic column breakthrough testing. Encouraged by the single-component gas sorption data, we performed dynamic column breakthrough (DCB) experiments on microcrystalline samples of **SOFOUR-2-Zn** and **SIFSIX-24-Zn**. A 1 : 1 C_2H_2/CO_2 mixture was passed through a column packed with activated sample under a total flow rate of 1.0 sccm and the effluent composition was monitored using mass spectrometry. For **SOFOUR-2-Zn** (Fig. 2e), CO_2 breakthrough occurred at 25.4 min g^{-1}, followed by C_2H_2 at 81.0 min g^{-1} (55.6 min g^{-1} later). During this interval, the minimum effluent purity of CO_2 was measured to be 99.989% and the saturation uptakes were 47.1 cm^3 g^{-1} and 23.2 cm^3 g^{-1} for C_2H_2 and CO_2, respectively, resulting in a separation factor (α_{AC}) of 2.05. For **SIFSIX-24-Zn** (Fig. 2f), CO_2 breakthrough occurred at 14.2 min g^{-1} with a minimum effluent purity of 99.991% and C_2H_2 breakthrough occurred at 78.6 min g^{-1} (64.4 min g^{-1} later). Minor fluctuations were observed at the onset of gas breakthrough in all experiments due to a pressure drop across the powdered sorbent bed. The saturation uptakes for C_2H_2 and CO_2 were determined to be 53.0 cm^3 g^{-1} and 10.1 cm^3 g^{-1}, respectively (Table S6†), resulting in higher α_{AC} of 5.26, putting **SIFSIX-24-Zn** in the same performance range as **TIFSIX-4-Cu** in terms of separation factor and pure component C_2H_2 uptake (5.4 and 3.85 mmol g^{-1}, respectively).[56]

Temperature Programmed Desorption (TPD) experiments were conducted after completion of the adsorption branches in DCB experiments for both **SOFOUR-2-Zn** and **SIFSIX-24-Zn** (Fig. 2g and h) by replacing the inlet gas mixture flow with 20

sccm of He and applying a temperature ramp of 5 °C min^{-1} from 25 °C to 60 °C. Desorption was continued until no further adsorbate was detected. We found that 60 °C was sufficient to regenerate both HUMs. Similar TPD curves were obtained for both **SOFOUR-2-Zn** and **SIFSIX-24-Zn**, characterised by rapid decreases in effluent CO_2 concentration, while C_2H_2 continued to be released with increasing temperature for a period prior to desorption. Fuel grade C_2H_2 (>98% purity) was eluted in the interval between 5 and 27 min g^{-1} for **SIFSIX-24-Zn**, and between 4 and 20 min g^{-1} for **SOFOUR-2-Zn**, corresponding to productivities of 9.45 L kg^{-1} and 7.69 L kg^{-1} of fuel grade C_2H_2 respectively, and peak C_2H_2 purities of 99.66 and 99.92%, respectively (Table S7†). These results are similar to literature values in terms of peak C_2H_2 purity for **TIFSIX-2-Cu-i**,[63] **SIFSIX-22-Zn** and **SOFOUR-1-Zn**,[22] which are all 99.9% or higher. The productivities for fuel grade C_2H_2 in a 1 : 1 C_2H_2/CO_2 mixture are 9.45 L kg^{-1} and 7.69 L kg^{-1} for **SIFSIX-24-Zn** and **SOFOUR-2-Zn**, respectively. This is much higher than previously reported values of 3.3 L kg^{-1} and 3.1 L kg^{-1}, for **SIFSIX-22-Zn** and **SOFOUR-1-Zn**, respectively.[22] **SOFOUR-2-Zn** and **SIFSIX-24-Zn** also produced significant amounts of high purity C_2H_2 (99.5%). For **SIFSIX-24-Zn**, >99.5% C_2H_2 eluted over the interval 5.8 to 23.9 min g^{-1}, resulting in a productivity of 8.75 L kg^{-1}, only 0.7 L kg^{-1} less than the production of fuel-grade >98% C_2H_2, but for **SOFOUR-2-Zn**, >99.5% C_2H_2 was eluted only between 5.3 and 9.4 min g^{-1} resulting in a significantly lower productivity of 3.01 L kg^{-1}. These values are lower than the benchmark of 53.8 L kg^{-1} for >99.5% C_2H_2 set by **ZNU-1**.[58] Additional DCB experiments conducted using a humid C_2H_2/CO_2 mixture showed that separation performance was largely unaffected by moisture in both **SOFOUR-2-Zn** and **SIFSIX-24-Zn** over a complete adsorption cycle, despite the poor stability of **SIFSIX-24-Zn** towards moisture (Fig. S18†).

Based on pure component isotherms and IAST calculations, both **SOFOUR-2-Zn** and **SIFSIX-24-Zn** should have roughly the same performance. However, DCB experiments revealed that despite showing comparable C_2H_2 uptakes in mixed-gas conditions, **SIFSIX-24-Zn** is better in terms of separation factor (2.05 *vs.* 5.26 for **SOFOUR-2-Zn** and **SIFSIX-24-Zn**, respectively). Production of high purity (>99.5%) C_2H_2 was also higher for **SIFSIX-24-Zn** than for **SOFOUR-2-Zn**, although, fuel-grade (>98%) productivity was similar for both. The differences might be attributed to the weaker Q_{st} for CO_2 of **SIFSIX-24-Zn**, 16.8 kJ mol^{-1} (ΔQ_{st} for $C_2H_2/CO_2 = 15.0$ kJ mol^{-1}), *vs.* 22.1 kJ mol^{-1} (ΔQ_{st} for $C_2H_2/CO_2 = 11.2$ kJ mol^{-1}) for **SOFOUR-2-Zn**.

Sorbate binding sites

To better understand the nature of the C_2H_2 and CO_2 binding sites, density functional theory (DFT) calculations were performed for **SOFOUR-2-Zn** and **SIFSIX-24-Zn** (see ESI† for computational methodology). In **SOFOUR-2-Zn**, the C_2H_2 molecule orients along one of the channel walls, forming simultaneous hydrogen bonds from both C–H hydrogen atoms to SO_4^{2-} oxygen atoms, with O···H distances of 2.57 Å and 2.62 Å (Fig. 3). In **SIFSIX-24-Zn**, hydrogen bonds are bifurcated, with the H-atoms being shared between two F-atoms of the same SIFSIX pillar, with distances of 2.38 and 2.66 Å on one end, and 2.93 Å with a contact of 3.66 Å on the other end (Fig. 3). These multi-site short contacts provide a clear basis for the selective C_2H_2 binding observed in both materials. In contrast, CO_2 binding sites are primarily governed by electrostatic interactions between the CO_2 carbon and electronegative pillar F and O atoms respectively (Fig. S19†). DFT-derived enthalpy values associated with gas adsorption are presented in Table S8.†

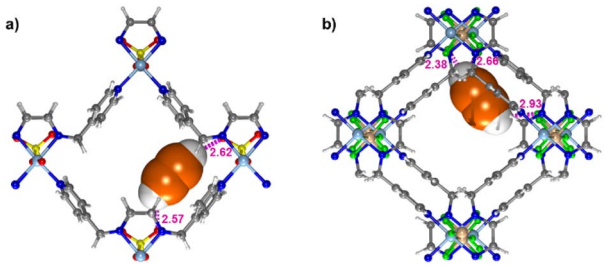

Fig. 3 Ball and stick models of (a) the C_2H_2 binding site for SOFOUR-2-Zn; (b) the C_2H_2 binding site for SIFSIX-24-Zn. Short contacts are highlighted as dashed magenta bonds and distances are given in Å.

Conclusions

The previously reported material $[Zn(\mathbf{enmepy})(SO_4)]_n$ (**SOFOUR-2-Zn**),[46] illustrates the potential utility of **en** based ligands for design of new HUMs with potential utility in gas separations. Pillar substitution using a crystal engineering approach enabled us to isolate $[Zn(\mathbf{enmepy})(SiF_6)]_n$ (**SIFSIX-24-Zn**), the prototypal member of a new platform of **MFSIX** HUMs. Pure component gas sorption studies and dynamic column breakthrough experiments revealed strong performance for the separation of C_2H_2 from CO_2 for both HUMs with appreciable amounts of fuel grade C_2H_2 (>98%) as shown by temperature programmed desorption of the sorbed gases from a 1 : 1 mixture of C_2H_2/CO_2. Productivities of 9.45 L kg^{-1} and 7.69 L kg^{-1} were measured for **SIFSIX-24-Zn** and **SOFOUR-2-Zn**, respectively, and **SIFSIX-24-Zn** produced high purity C_2H_2 (>99.5%). This study demonstrates for the first time that chelating ethylenediamine based ligands can sustain facile to synthesise HUMs with strong gas separation properties. Both HUM platforms are inherently modular and their scope in terms of composition and properties are under further investigation in our laboratory. We anticipate that **SIFSIX-24-Zn** and **SOFOUR-2-Zn** will serve as prototypes for families of second-generation sorbents through metal and/or pillar substitution, as well as ligand modification.

Data availability

The data supporting the findings of this study are available in the ESI† or from the authors upon request.

Author contributions

Project conceptualisation: D. J. O., D. S., S. M. and M. J. Z.; synthesis and characterisation: D. J. O., A. R. and A. A. B.; single component gas sorption: D. S., A. R. and D. J. O.; dynamic

column breakthrough and temperature programmed desorption: D. S. and S. M.; molecular modelling: M. V.; single crystal X-ray crystallography: D. J. O.; Cambridge Structural Database analysis: D. J. O. and A. R.; writing – original draft: D. J. O., D. S., S. M., A. A. B., and M. J. Z.; writing – review & editing: all authors; funding acquisition: M. J. Z. and M. V.; supervision: S. M., M. J. Z. and M. V. D. J. O., D. S. and A. R. contributed equally to this work.

Conflicts of interest

There are no conflicts to declare.

Acknowledgements

We gratefully acknowledge Science Foundation Ireland (16/IA/4624, and 12/RC/2278_P2) and the European Research Council (ADG885695). M. V. acknowledges the Irish Centre for High-End Computing (ICHEC) for the provision of computational facilities and support. Amin Koochaki is acknowledged for useful discussions and preliminary modelling studies. S. M. acknowledges an SFI-IRC Pathway award (21/PATH-S/9454) from the Science Foundation Ireland.

Notes and references

1 W. Mori, F. Inoue, K. Yoshida, H. Nakayama, S. Takamizawa and M. Kishita, *Chem. Lett.*, 1997, **26**, 1219–1220.
2 M. Kondo, T. Yoshitomi, H. Matsuzaka, S. Kitagawa and K. Seki, *Angew. Chem., Int. Ed.*, 1997, **36**, 1725–1727.
3 H. Li, M. Eddaoudi, T. L. Groy and O. M. Yaghi, *J. Am. Chem. Soc.*, 1998, **120**, 8571–8572.
4 X. Zhao, Y. Wang, D.-S. Li, X. Bu and P. Feng, *Adv. Mater.*, 2018, **30**, 1705189.
5 J.-R. Li, R. J. Kuppler and H.-C. Zhou, *Chem. Soc. Rev.*, 2009, **38**, 1477–1504.
6 S. Mukherjee, D. Sensharma, K.-J. Chen and M. J. Zaworotko, *Chem. Commun.*, 2020, **56**, 10419–10441.
7 L. Yang, S. Qian, X. Wang, X. Cui, B. Chen and H. Xing, *Chem. Soc. Rev.*, 2020, **49**, 5359–5406.
8 G. Verma, J. Ren, S. Kumar and S. Ma, *Eur. J. Inorg. Chem.*, 2021, **2021**, 4498–4507.
9 D. Zhao, K. Yu, X. Han, Y. He and B. Chen, *Chem. Commun.*, 2022, **58**, 747–770.
10 P. Nugent, Y. Belmabkhout, S. D. Burd, A. J. Cairns, R. Luebke, K. Forrest, T. Pham, S. Ma, B. Space, L. Wojtas, M. Eddaoudi and M. J. Zaworotko, *Nature*, 2013, **495**, 80–84.
11 S. Mukherjee and M. J. Zaworotko, *Trends Chem.*, 2020, **2**, 506–518.
12 K. Uemura, A. Maeda, T. K. Maji, P. Kanoo and H. Kita, *Eur. J. Inorg. Chem.*, 2009, **2009**, 2329–2337.
13 A. Kumar, C. Hua, D. G. Madden, D. O'Nolan, K.-J. Chen, L.-A. J. Keane, J. J. Perry and M. J. Zaworotko, *Chem. Commun.*, 2017, **53**, 5946–5949.
14 S. Mukherjee, N. Kumar, A. A. Bezrukov, K. Tan, T. Pham, K. A. Forrest, K. A. Oyekan, O. T. Qazvini, D. G. Madden, B. Space and M. J. Zaworotko, *Angew. Chem., Int. Ed.*, 2021, **60**, 10902–10909.
15 N. C. Harvey-Reid, D. Sensharma, S. Mukherjee, K. M. Patil, N. Kumar, S. J. Nikkhah, M. Vandichel, M. J. Zaworotko and P. E. Kruger, *ACS Appl. Mater. Interfaces*, 2024, **16**, 4803–4810.
16 H. S. Scott, A. Bajpai, K.-J. Chen, T. Pham, B. Space, J. J. Perry and M. J. Zaworotko, *Chem. Commun.*, 2015, **51**, 14832–14835.
17 H. S. Scott, N. Ogiwara, K.-J. Chen, D. G. Madden, T. Pham, K. Forrest, B. Space, S. Horike, J. J. Perry Iv, S. Kitagawa and M. J. Zaworotko, *Chem. Sci.*, 2016, **7**, 5470–5476.
18 P. M. Bhatt, Y. Belmabkhout, A. Cadiau, K. Adil, O. Shekhah, A. Shkurenko, L. J. Barbour and M. Eddaoudi, *J. Am. Chem. Soc.*, 2016, **138**, 9301–9307.
19 A. Cadiau, K. Adil, P. M. Bhatt, Y. Belmabkhout and M. Eddaoudi, *Science*, 2016, **353**, 137–140.
20 A. Cadiau, Y. Belmabkhout, K. Adil, P. M. Bhatt, R. S. Pillai, A. Shkurenko, C. Martineau-Corcos, G. Maurin and M. Eddaoudi, *Science*, 2017, **356**, 731–735.
21 M. H. Mohamed, S. K. Elsaidi, T. Pham, K. A. Forrest, B. Tudor, L. Wojtas, B. Space and M. J. Zaworotko, *Chem. Commun.*, 2013, **49**, 9809–9811.
22 D. Sensharma, D. J. O'Hearn, A. Koochaki, A. A. Bezrukov, N. Kumar, B. H. Wilson, M. Vandichel and M. J. Zaworotko, *Angew. Chem., Int. Ed.*, 2022, **61**, e202116145.
23 J. Wang, Y. Zhang, Y. Su, X. Liu, P. Zhang, R.-B. Lin, S. Chen, Q. Deng, Z. Zeng, S. Deng and B. Chen, *Nat. Commun.*, 2022, **13**, 200.
24 R.-B. Lin, L. Li, H. Wu, H. Arman, B. Li, R.-G. Lin, W. Zhou and B. Chen, *J. Am. Chem. Soc.*, 2017, **139**, 8022–8028.
25 H. S. Scott, M. Shivanna, A. Bajpai, D. G. Madden, K.-J. Chen, T. Pham, K. A. Forrest, A. Hogan, B. Space, J. J. Perry Iv and M. J. Zaworotko, *ACS Appl. Mater. Interfaces*, 2017, **9**, 33395–33400.
26 M. Shivanna, K.-i. Otake, B.-Q. Song, L. M. van Wyk, Q.-Y. Yang, N. Kumar, W. K. Feldmann, T. Pham, S. Suepaul, B. Space, L. J. Barbour, S. Kitagawa and M. J. Zaworotko, *Angew. Chem., Int. Ed.*, 2021, **60**, 20383–20390.
27 S. K. Elsaidi, M. H. Mohamed, T. Pham, T. Hussein, L. Wojtas, M. J. Zaworotko and B. Space, *Cryst. Growth Des.*, 2016, **16**, 1071–1080.
28 Q. Lin, C. Mao, A. Kong, X. Bu, X. Zhao and P. Feng, *J. Mater. Chem. A*, 2017, **5**, 21189–21195.
29 L. He, J. K. Nath and Q. Lin, *Chem. Commun.*, 2019, **55**, 412–415.
30 Q.-L. Qian, X.-W. Gu, J. Pei, H.-M. Wen, H. Wu, W. Zhou, B. Li and G. Qian, *J. Mater. Chem. A*, 2021, **9**, 9248–9255.
31 S. Zou, Z. Di, Y. Liu, Z. Ji, H. Li, C. Chen and M. Wu, *Inorg. Chem. Commun.*, 2022, **137**, 109198.
32 Y. Liu, Y. Zhang, P. Zhang, Y. Peng, X. Liu, J. Chen, S. Chen, Z. Zeng, J. Wang and S. Deng, *Chem. Eng. Process.*, 2022, **172**, 108768.
33 J. Liu, H. Shuai, J. Chen, S. Chen, Z. Zhou, J. Wang and S. Deng, *Chem & Bio Eng.*, 2024, **1**, 83–90.

34 D. Sensharma, B. H. Wilson, N. Kumar, D. J. O'Hearn and M. J. Zaworotko, *Cryst. Growth Des.*, 2022, **22**, 5472–5480.
35 Y. H. Andaloussi, D. Sensharma, A. A. Bezrukov, D. C. Castell, T. He, S. Darwish and M. J. Zaworotko, *Cryst. Growth Des.*, 2024, **24**, 2573–2579.
36 X. Liu, P. Zhang, H. Xiong, Y. Zhang, K. Wu, J. Liu, R. Krishna, J. Chen, S. Chen, Z. Zeng, S. Deng and J. Wang, *Adv. Mater.*, 2023, **35**, 2210415.
37 C. R. Groom, I. J. Bruno, M. P. Lightfoot and S. C. Ward, *Acta Crystallogr., Sect. B: Struct. Sci., Cryst. Eng. Mater.*, 2016, **72**, 171–179.
38 J. Haníková, J. Černák, J. Kuchár and E. Čižmár, *Inorg. Chim. Acta*, 2012, **385**, 178–184.
39 J. Lhoste, K. Adil, A. Le Bail, M. Leblanc, A. Hémon-Ribaud and V. Maisonneuve, *J. Fluor. Chem.*, 2012, **134**, 29–34.
40 P. C. Healy, C. H. L. Kennard, G. Smith and A. H. White, *Cryst. Struct. Commun.*, 1978, **7**, 565–570.
41 V. Manríquez, M. Campos-Vallette, N. Lara, N. González-Tejeda, O. Wittke, G. Díaz, S. Diez, R. Muñoz and L. Kriskovic, *J. Chem. Crystallogr.*, 1996, **26**, 15–22.
42 M. K. Taylor, D. E. Stevenson, L. E. A. Berlouis, A. R. Kennedy and J. Reglinski, *J. Inorg. Biochem.*, 2006, **100**, 250–259.
43 O. V. Kravchina, A. I. Kaplienko, E. P. Nikolova, A. G. Anders, D. V. Ziolkovskii, A. Orendachova and M. Kajnakova, *Russ. J. Phys. Chem.*, 2011, **5**, 209–214.
44 M. Lutz, S. Smeets and P. Parois, *Acta Crystallogr., Sect. E: Crystallogr. Commun.*, 2010, **66**, m671–m672.
45 M. Kajňaková, A. Orendáčová, M. Orendáč, A. Feher, M. Mal'arová and Z. Trávníček, *Acta Phys. Pol.*, 2008, **113**, 507–510.
46 Y. Wen, T. Sheng, Z. Sun, Z. Xue, Y. Wang, Y. Wang, S. Hu, X. Ma and X. Wu, *Chem. Commun.*, 2014, **50**, 8320–8323.
47 Y. Wen, T. Sheng, X. Zhu, C. Zhuo, S. Su, H. Li, S. Hu, Q.-L. Zhu and X. Wu, *Adv. Mater.*, 2017, **29**, 1700778.
48 S. Khatua, A. Santra, S. Padmakumar, K. Tomar and S. Konar, *ChemistrySelect*, 2018, **3**, 785–793.
49 C. F. Macrae, I. Sovago, S. J. Cottrell, P. T. A. Galek, P. McCabe, E. Pidcock, M. Platings, G. P. Shields, J. S. Stevens, M. Towler and P. A. Wood, *J. Appl. Crystallogr.*, 2020, **53**, 226–235.
50 A. Spek, *Acta Crystallogr., Sect. C: Struct. Chem.*, 2015, **71**, 9–18.
51 Y. Wen, T. Sheng, S. Hu, X. Ma, C. Tan, Y. Wang, Z. Sun, Z. Xue and X. Wu, *Chem. Commun.*, 2013, **49**, 10644–10646.
52 Y. Wen, T. Sheng, S. Hu, Y. Wang, C. Tan, X. Ma, Z. Xue, Y. Wang and X. Wu, *CrystEngComm*, 2013, **15**, 2714–2721.
53 Y. Wen, T. Sheng, C. Zhuo, X. Zhu, S. Hu, W. Cao, H. Li, H. Zhang and X. Wu, *Inorg. Chem.*, 2016, **55**, 4199–4205.
54 A. Nuhnen and C. Janiak, *Dalton Trans.*, 2020, **49**, 10295–10307.
55 N. Kumar, S. Mukherjee, N. C. Harvey-Reid, A. A. Bezrukov, K. Tan, V. Martins, M. Vandichel, T. Pham, L. M. van Wyk, K. Oyekan, A. Kumar, K. A. Forrest, K. M. Patil, L. J. Barbour, B. Space, Y. Huang, P. E. Kruger and M. J. Zaworotko, *Chem*, 2021, **7**, 3085–3098.
56 D. M. Venturi, M. S. Notari, R. Bondi, E. Mosconi, W. Kaiser, G. Mercuri, G. Giambastiani, A. Rossin, M. Taddei and F. Costantino, *ACS Appl. Mater. Interfaces*, 2022, **14**, 40801–40811.
57 C. M. Simon, B. Smit and M. Haranczyk, *Comput. Phys. Commun.*, 2016, **200**, 364–380.
58 L. Wang, W. Sun, Y. Zhang, N. Xu, R. Krishna, J. Hu, Y. Jiang, Y. He and H. Xing, *Angew. Chem., Int. Ed.*, 2021, **60**, 22865–22870.
59 Y. Chen, Y. Du, Y. Wang, R. Krishna, L. Li, J. Yang, J. Li and B. Mu, *AIChE J.*, 2021, **67**, e17152.
60 N. Kumar, S. Mukherjee, A. A. Bezrukov, M. Vandichel, M. Shivanna, D. Sensharma, A. Bajpai, V. Gascón, K.-i. Otake, S. Kitagawa and M. J. Zaworotko, *SmartMat*, 2020, **1**, e1008.
61 L. Zhang, K. Jiang, J. Zhang, J. Pei, K. Shao, Y. Cui, Y. Yang, B. Li, B. Chen and G. Qian, *ACS Sustain. Chem. Eng.*, 2019, **7**, 1667–1672.
62 M. Jiang, X. Cui, L. Yang, Q. Yang, Z. Zhang, Y. Yang and H. Xing, *Chem. Eng. J.*, 2018, **352**, 803–810.
63 K.-J. Chen, H. S. Scott, D. G. Madden, T. Pham, A. Kumar, A. Bajpai, M. Lusi, K. A. Forrest, B. Space, J. J. I. V. Perry and M. J. Zaworotko, *Chem*, 2016, **1**, 753–765.